

Zebrafish B cell acute lymphoblastic leukemia: new findings in an old model

Gilseung Park^{1,*}, Jessica Burroughs-Garcia^{2,*}, Clay A. Foster^{3,*}, Ameera Hasan⁴, Chiara Borga² and J. Kimble Frazer^{1,2,4}

¹Department of Cell Biology, University of Oklahoma Health Sciences Center, Oklahoma City, OK 73104, USA

²Department of Pediatrics, Section of Pediatric Hematology-Oncology, University of Oklahoma Health Sciences Center, Oklahoma City, OK 73104, USA

³Department of Microbiology and Immunology, University of North Carolina, Chapel Hill, NC 27599, USA

⁴Department of Microbiology & Immunology, University of Oklahoma Health Sciences Center, Oklahoma City, OK 73104, USA

*These authors contributed equally to this work

Correspondence to: J. Kimble Frazer, **email:** Kimble-Frazer@ouhsc.edu

Keywords: acute lymphoblastic leukemia; ALL; zebrafish; lymphocyte; MYC

Received: November 13, 2019

Accepted: March 19, 2020

Published: April 14, 2020

Copyright: Park et al. This is an open-access article distributed under the terms of the Creative Commons Attribution License 3.0 (CC BY 3.0), which permits unrestricted use, distribution, and reproduction in any medium, provided the original author and source are credited.

ABSTRACT

Acute lymphoblastic leukemia (ALL) is the most common pediatric, and ninth most common adult, cancer. ALL can develop in either B or T lymphocytes, but B-lineage ALL (B-ALL) exceeds T-ALL clinically. As for other cancers, animal models allow study of the molecular mechanisms driving ALL. Several zebrafish (*Danio rerio*) T-ALL models have been reported, but until recently, robust *D. rerio* B-ALL models were not described. Then, *D. rerio* B-ALL was discovered in two related zebrafish transgenic lines; both were already known to develop T-ALL. Here, we report new B-ALL findings in one of these models, fish expressing transgenic human *MYC* (*hMYC*). We describe B-ALL incidence in a large cohort of *hMYC* fish, and show B-ALL in two new lines where T-ALL does not interfere with B-ALL detection. We also demonstrate B-ALL responses to steroid and radiation treatments, which effect ALL remissions, but are usually followed by prompt relapses. Finally, we report gene expression in zebrafish B lymphocytes and B-ALL, in both bulk samples and single B- and T-ALL cells. Using these gene expression profiles, we compare differences between the two new *D. rerio* B-ALL models, which are both driven by transgenic mammalian *MYC* oncoproteins. Collectively, these new data expand the utility of this new vertebrate B-ALL model.

INTRODUCTION

Acute lymphoblastic leukemia (ALL) and the related malignancy lymphoblastic lymphoma (LBL) dominate pediatric oncology, together representing over one third of all childhood cancer [1–3]. These diseases afflict even more adults in absolute terms, and are more often fatal in them [4, 5]. ALL and LBL can develop in lymphoblasts of either the B or T cell lineage; B-ALL exceeds T-ALL, but T-LBL is more prevalent than B-LBL. Despite treatments for these diseases improving considerably over the past several decades, relapsed ALL is actually the 4th most-frequent pediatric cancer diagnosis and second most lethal childhood malignancy, accounting for ~25% of all deaths [6–8].

Animal studies have been instrumental in investigating the genetics, genomics, drug sensitivities, and other features of ALL and LBL, and several mouse models for these diseases exist [9, 10]. Mammalian systems have advantages such as anatomic, physiologic, and genetic conservation, with mice being the main mammal utilized, but other organisms provide complementary advantages. Zebrafish (*Danio rerio*) offer flexible genetic tools, powerful live imaging, high fecundity, rapid development, shared oncogenic pathways, affordability, and other favorable traits that have allowed them to quickly gain traction as a cancer model [11–17].

Many groups have exploited these attributes to create zebrafish leukemia models, specifically for acute

myeloid leukemia (AML) and T-ALL [18–37]. For T-ALL in particular, zebrafish models have been highly informative, advancing our understanding of T-ALL genetics, pro- and anti-oncogenic interactions between different genes and pathways, tumor heterogeneity, leukemia stem cells, and in screens for new therapeutics [28, 38–53]. However, despite the fact that zebrafish T-ALL models had proven to be fertile grounds for study, B-ALL modeling in *D. rerio* had not been fruitful, with only one low penetrance and long latency line reported [54]. This was curious because a zebrafish *recombination activating gene 2* (*rag2*) promoter—active in both immature T and B cells—was used to regulate most of these transgenic oncoproteins in the various T-ALL lines, yet *D. rerio* B-ALL had not been reported in them [55, 56]. Overall, since B-ALL is the more prevalent type in patients, the lack of B-lineage models was particularly unfortunate.

In 2018, the zebrafish ALL field advanced suddenly with reports of B-ALL in two closely-related transgenic lines where T-ALL was already known to occur [57, 58]. In one, a *rag2:mMyc* (murine *Myc*) transgene was used [29], with ALL purified as single clones by allo-transplantation. Two of 12 ALL analyzed by RNA sequencing (RNA-seq) exhibited gene expression consistent with B-ALL cells arrested at the pro-B cell stage [57]. In the other, a *rag2:hMYC* (human *MYC*) transgene was utilized [32], as well as a transgenic marker, *lck:eGFP* [59], differentially expressed by B and T cells. Analysis of over one hundred animals demonstrated that many develop B-ALL, others develop T-ALL (as previously known), and still other fish acquire both ALL types concomitantly [58]. A follow-up report by these groups further showed that despite high similarity between the *mMyc* and *hMYC* transgenes used, these B-ALL are actually quite different, occurring in distinct B cell lineages and with dissimilar expression patterns [60]. Here, we present new results in the *hMYC* model, including B- and T-ALL latency and penetrance data in a cohort of over 600 animals, *in vivo* glucocorticoid and radiation treatment of B-ALL, and expression profiles from single B- and T-ALL cells. We also present new analyses that compare *mMyc* vs. *hMYC* B-ALL to reveal key biologic pathways that distinguish them.

MATERIALS AND METHODS

Zebrafish care

Zebrafish care was provided as previously reported [58]. Animals were housed in an aquatic colony at 28.5°C on a 14:10 hour light:dark circadian cycle and experiments performed according to protocols approved by the University of Oklahoma Health Sciences Center IACUC (12-066 and 15-046). For all procedures, fish were anesthetized with 0.02% tricaine methanesulfonate (MS-222). *D. rerio* with the *cd79a:GFP* or *cd79b:GFP*

transgenic markers [61] were bred to *rag2:hMYC* fish [32] to create the new transgenic lines reported herein.

Fluorescent microscopy

Anesthetized 3–9 month old *hMYC; GFP* fish were screened for abnormal GFP patterns using a Nikon AZ100 fluorescent microscope. Low exposure (200 ms, 2.8× gain) and high exposure (1.5 s, 3.4× gain) settings were used to obtain images with Nikon DS-Qi1MC camera. Images were processed with Nikon NIS Elements Version 4.13 software.

Fluorescence-Activated Cell Sorting (FACS) and flow cytometric analyses

As previously described [58], cells from whole fish were dissociated using a pestle, and then passed through 35 µm filters. GFP^{hi}, GFP^{lo}, and/or GFP⁻ cells were collected from the lymphoid and precursor gates using a BD-FACSJazz Instrument (Becton Dickinson, San Jose, CA, USA). Flow cytometric analyses were performed using FlowJo software (Ashland, OR, USA).

B- and T-ALL incidence studies

Beginning at ~75 dpf, a cohort of 628 *rag2:hMYC;lck:GFP* zebrafish was monitored by ~weekly fluorescence microscopy to detect ALL. Animals that developed fluorescent cancers were euthanized and single cell suspensions were prepared as described previously [58]. Cells in the lymphoid and precursor gates were analyzed for GFP intensity using a Beckman-Coulter CytoFLEX™ to determine whether each ALL derived from T, B, or both lymphocyte lineages [58, 62, 63].

In vivo dexamethasone and radiation treatments of *D. rerio* B-ALL

Zebrafish with B-ALL were treated by continuous immersion in 5 µg/ml dexamethasone (DXM) in normal fish water for 9 days, modified from our prior zebrafish T-ALL DXM protocol [43, 64]. Water and DXM were changed daily, with one or two fish housed in 500 ml. After completing treatment, animals were monitored by weekly fluorescent microscopy to detect relapse. Zebrafish with B-ALL were treated by γ -irradiation (IR) using a Cesium¹³⁷ irradiator to deliver a total dose of 15 Gy divided in two fractions: 10 Gy on day 0 and a 5 Gy boost on day 5. Animals were imaged by fluorescent microscopy prior to treatment, 2 days post-treatment (day 7), and weekly-to-monthly thereafter to monitor for relapse.

Nanostring™ gene expression analyses

FACS purification of normal lymphocyte and ALL samples from WT and *rag2:hMYC* fish, RNA extraction,

and probe hybridization were performed as described previously [58], with gene identities and probe sequences available in the online supplemental material of that publication. Hybridization data were analyzed using nSolver 3.0 software (Nanostring nCounter Technologies, Seattle, WA, USA). Read counts were log-transformed and converted to z-scores for visualization purposes.

Single-cell qRT-PCR analyses of *hMYC* B- and T-ALL

ALL cells from double-transgenic *hMYC* fish were isolated from peritoneal washings as described previously [63]. Individual B- and T-ALL cells were FAC-sorted into 96 well plates, and cells were lysed, RNA extracted, and cDNA synthesized according to the Fluidigm™ single-cell protocol. Twenty-cycle pre-amplification reactions were performed using gene-specific primers (listed in Supplementary Table 1.) according to manufacturer instructions. Unincorporated primers were digested with exonuclease I (NEB M0293L) and samples diluted 5-fold in DNA suspension buffer (TEKnova PN T0221). Single-cell pre-amplified cDNA were then quantified by qRT-PCR in a Fluidigm BioMark HD machine using 48.48 Dynamic Array Chips for Gene Expression following the manufacturer's protocol. CT values were converted to Log2Ex values for visualization purposes using a limit of detection (LoD) of 28. Additional LoD limits were examined and showed similar results.

RNA-seq and gene expression comparisons of *hMYC* and *mMyc* B-ALL

Paired-end RNA-seq reads were trimmed with BBduk (v.38.22; retrieved from <http://sourceforge.net/projects/bbmap>) and aligned to the *D. rerio* GRCz11 genome using STAR (v.2.6.1b; default settings optimized for read-length) [65]. Picard's MarkDuplicates tool (v.2.18.14; retrieved from <http://broadinstitute.github.io/picard>) was used to identify potential duplicates. Gene counts were generated with featureCounts (RSubread v.1.32.1) using *D. rerio* Ensembl annotation (release 92) [66, 67]. Ribosomal and mitochondrial RNA were excluded. Counts were processed and normalized within DESeq2 (v.1.22.1) [68], and pairwise differential expression testing was used to compare *hMYC* and *mMyc* B-ALL (adjusted *p*-value < 0.05, absolute fold-change > 1.5). Additional filtering steps were as described previously [60]. Putative human orthologues were mapped to corresponding *D. rerio* genes using BEAGLE (update 090718; retrieved from <http://chgr.mgh.harvard.edu/genomesrus/index.php>). In downstream analyses, a gene count threshold of 100 was used for each up-regulated group (minimum expression in at least 75% of in-group samples). RNA-seq heatmaps depict normalized counts

generated via the variance-stabilizing transformation in DESeq2, unless otherwise described. Over-representation analysis was performed with clusterProfiler (v.3.10.0) [69] using putative human orthologues (FDR < 0.05) in the C2, C5, and C7 collections from MSigDB (v.7.0) [70]. The 10 highest-scoring pathways by FDR *q*-value for each group were chosen for visualization, with pathway names changed for brevity. Highly-redundant pathways were excluded manually, based on gene overlap. Original pathway names (order matching Figure 6B) and related data are listed in Supplementary Table 4.

RESULTS AND DISCUSSION

B-ALL is early onset and highly penetrant in *hMYC* zebrafish

We previously analyzed more than 50 unique *hMYC* B-ALL [58, 60], demonstrating these fish are a robust model, but latency and incidence rates for B- and T-ALL have not been reported in the *hMYC* line. To determine these, beginning at 3 months of age, we monitored fish by serial fluorescent microscopy to detect GFP^{lo} B-ALL and GFP^{hi} T-ALL, as we described previously (Figure 1A) [58]. Using the *lck:GFP* marker, GFP^{lo} B-ALL fluoresce dimly, making them difficult to discern by microscopy and more likely to require high disease burdens to be detected. In addition, brightly fluorescent T-ALL can obscure detection of B-ALL. To address these possibilities, we flow cytometrically tested ALL in order to definitively assign them to the correct group.

We surveyed over 600 fish until 184 days post fertilization (dpf) and found ~60% developed at least one form of ALL by that time (Figure 1A). Isolated T-ALL was most common (40%), with peak incidence between 4-5 months. B-ALL followed a similar time course, with 12% incidence by 184 dpf, and another 7% of animals developing both T- and B-ALL. To confirm these results, every ALL was analyzed flow cytometrically (Figure 1B). By 300 dpf, every surviving animal had developed at least one type of ALL (64% T-ALL, 23% B-ALL, 13% T- and B-ALL; data not shown). We conclude that ALL is highly penetrant in *hMYC* fish, with peak onset beginning shortly after 120 dpf.

To simplify detection of B-ALL by fluorescent microscopy and eliminate the need for flow cytometric confirmation, we created double-transgenic fish with *rag2:hMYC* and either the *cd79a:GFP* or *cd79b:GFP* marker (Figure 1C), which utilize promoters from B cell-specific proteins that are components of the surface immunoglobulin signaling complex [61]. In these lines, B-ALL fluoresce brightly, but T-ALL do not fluoresce. These models will be useful for B-ALL studies, particularly in investigations with potential therapeutic agents. The highly-fluorescent B-ALL of these lines can facilitate accurate and high-throughput determinations of

both response rates and relapse kinetics, allowing precise regression measurements via fluorescence quantifications, and more sensitive detection of B-ALL relapses when disease burden still remains low.

B-ALL respond to dexamethasone and radiation treatments

The glucocorticoids prednisone and dexamethasone (DXM) are the backbone of ALL therapy in patients, and γ -irradiation (IR) remains an effective adjunct that is also used, although it is reserved for specific cases

due to toxicity [71, 72]. To determine whether B-ALL in zebrafish are similarly responsive to these modalities and establish protocols for future therapeutic studies in this model, we devised *in vivo* regimens for DXM and IR treatment of *D. rerio* with B-ALL.

For DXM, fish were housed continuously in fish water containing 5 $\mu\text{g/ml}$ DXM for 9 days, modified from our prior DXM studies in zebrafish T-ALL, and monitored by serial fluorescence microscopy [43, 64]. We treated nineteen animals, and every B-ALL showed robust regression, with most becoming undetectable by fluorescent microscopy by the end of treatment

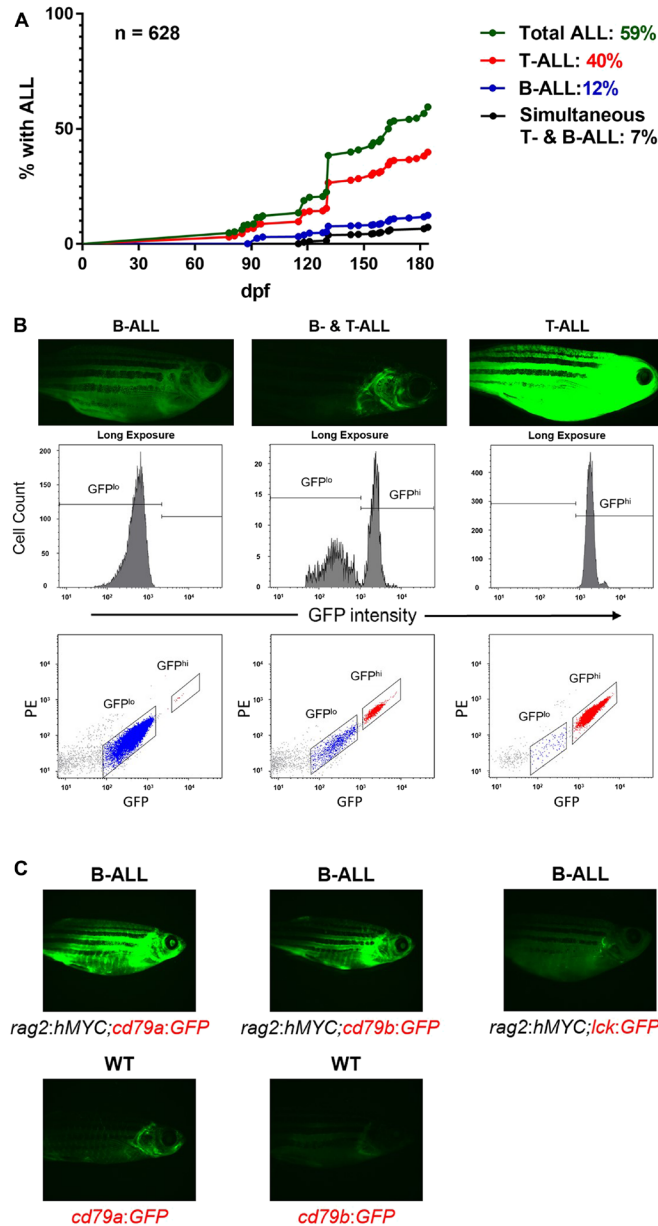


Figure 1: B-ALL in *hMYC* zebrafish. (A) Curves displaying B- and T-ALL incidence by 184 dpf, as determined by fluorescence microscopy. (B) Fluorescence microscopy images of fish with B-ALL (left), both B- and T-ALL (center), or T-ALL (right). Flow cytometry plots of ALL samples from these fish are shown beneath them. (C) B-ALL appearance in fish with *rag2:hMYC* and different transgenic markers: *cd79a:GFP* (left), *cd79b:GFP* (center), or *lck:GFP* (right). WT *cd79a:GFP* or *cd79b:GFP* fish without B-ALL are shown beneath for comparison. Images are representative of > 50 animals examined for each genotype.

(Figure 2A). After completing DXM treatment, we then monitored fish for 9 weeks, with 58% (11/19) recurring by 4 weeks. We conclude that our DXM protocol effectively kills most B-ALL cells, as 100% of animals exhibited brisk responses, but in many cases, sufficient B-ALL cells persist to re-grow the cancer quickly. Based on this, we believe this model can be utilized to investigate the genetic and molecular features of steroid-resistant ALL, a significant clinical problem in ALL patients [73].

IR is toxic in patients, and we also observed this in zebrafish with B-ALL. We initially administered IR treatments of 20 Gray (Gy) as single doses, but many animals died, despite the fact that this dose is well-tolerated by wild-type (WT) fish [59]. To diminish IR toxicity, presumably caused by overwhelming tumor lysis [74], we divided IR into two fractions, giving 10 Gy on day 0 and an additional 5 Gy on day 5. This was better tolerated, and following the second fraction, B-ALL were undetectable by fluorescence microscopy (Figure 2B). However, as seen in many DXM-treated B-ALL, all B-ALL relapsed post-IR, and recurrences were even more rapid (~3 weeks). From these results, we infer that IR (like DXM) kills most B-ALL cells, but surviving cells quickly re-populate the tumor. In addition, the rapid re-growth of B-ALL after IR suggests either more cells persist following IR, or that B-ALL cells that survive IR adopt more aggressive phenotypes. Distinguishing between these possibilities and unravelling the underlying mechanisms responsible will be informative to the clinical scenarios these experiments represent.

Defining B-ALL and B cell gene expression patterns

We discovered many *D. rerio* B lymphocytes and B-ALL express low levels of *lck* [58], which fostered new studies not previously done in zebrafish, such as FACS isolation of B-lineage cells (i. e., GFP^{lo} cells from *lck:GFP* fish) and profiling their gene expression [58, 63]. These findings translate to humans because immature human B cells and many patients' B-ALL also express low levels of *LCK* [58, 75, 76]. It is currently not known if these newly-described *lck*^{lo}/*LCK*^{lo} B cells represent one, or many, B cell population(s).

To begin to address this, we assessed gene expression in lymphocytes of fish carrying only the *lck:GFP* marker transgene (henceforth referred to as WT) and double-transgenic *rag2:hMYC, lck:GFP* fish (henceforth, *hMYC*). We FACS-purified lymphoid gate cells from both marrow and thymus, and further divided these into GFP-negative (GFP⁻), GFP^{lo}, and GFP^{hi} fractions [58, 62]. We then used NanostringTM, a multiplexed probe-based hybridization technique, to quantify mRNAs expressed by each population [77, 78]. To categorize distinct cell identities, we selected zebrafish gene homologues whose expression distinguishes mammalian B, T, and other leukocytes for

these experiments [58, 79]. We found that GFP^{hi} cells from both thymus and marrow in both genotypes (WT, *hMYC*) express T-lineage transcripts such as *cd2, cd4, cd8a, itk, lat*, and T cell receptor (TCR) mRNA (*trcd, trcg, trbc2, trac, trbc1*; Figure 3A). RNA-seq studies by other groups indicate some *D. rerio* natural killer (NK) and myeloid cells also express *lck* [49, 80], but transcripts indicative of these cells were not seen, suggesting they are minor populations in marrow and thymus. In contrast, B cell gene expression (*cd79a, cd79b, ighz, btk, cd22, syk, lyn, pax5, blnk, ighm*, etc.) was prominent in GFP^{lo} and GFP⁻ fractions from both organs (Figure 3A), particularly in *hMYC* GFP^{lo} cells of both marrow (Figure 3B) and thymus (Figure 3C), where B-lineage genes were the dominant signature. We draw two inferences from these data: (1) *lck* and *lck*^{lo} lymphocytes both contain B cells, but the *lck*^{lo} population has greater B cell enrichment and (2) *lck*^{lo} B cells are more abundant in *hMYC* fish, as B-lineage genes were more dominant in *hMYC* GFP^{lo} signatures than in those of WT animals.

These results support our conclusions, but using bulk gene expression patterns to compare populations that contain multiple cell types is challenging. Alternatively, single cell analyses can unambiguously define cell identities and precisely quantify different cell types. Such approaches can also reveal heterogeneity in seemingly-uniform populations, which is more powerful than binary categorizations like simple lineage assignments. Recognizing differences between cells of the same lineage, or cells of the same cancer, also has functional relevance, since distinct gene expression patterns correspond to different cellular phenotypes. Lymphocytes are diverse and complex populations, composed of not only B, T, and NK cells, but also innate lymphoid cells (ILC) [81]. Moreover, each of these cell types have multiple additional subtypes, such as the distinct IgM and IgZ B cell lineages in teleost fish [61, 82–84] or the various T lymphocyte subtypes [e. g., cytotoxic (CD8⁺ CTL), helper (CD4⁺ T_H), T_H 17, and regulatory (T_{reg}) subclasses] [85–87].

Diversity is not unique to normal lymphocytes; lymphoid cancers also contain heterogeneous populations, as previously shown in *D. rerio* *mMyc*-driven T-ALL [15, 40, 45, 48]. To assess tumor heterogeneity in *hMYC*-induced ALL and begin to define its extent, we analyzed mRNA expression in single cells from B- or T-ALL from *hMYC* fish (Figure 4). Animals exhibited either dim or bright cancers by fluorescent microscopy (Figure 4A) and by FACS analysis (Figure 4B). Using Fluidigm BiomarkTM multiplex quantitative reverse transcriptase polymerase chain reaction (PCR primers are listed in Supplementary Table 1), we analyzed the expression of 17 transcripts: 10 B-lineage, 6 T-lineage, and as a mRNA threshold control, *eukaryotic translation elongation factor 1 alpha 1, like 1 (ef1a)* in 10 B- and 10 T-ALL individual cells (Figure 4C). All 20 B- and T-ALL cells profiled in accordance with their expected lineage, but expression differences of

specific genes in single cells (e. g., *pax5*, *id3*, etc.) were evident. In addition, select genes (e. g., *foxo1b*, *skap1*) occasionally were mis-expressed by cells of the ‘wrong’ lineage. The significance of these findings remain to be determined, as malignant cells express aberrant markers on occasion [88], but biphenotypic ALL was demonstrated in *mMyc* fish, so what has previously been termed gene ‘mis-expression’ may actually represent an intriguing finding [57, 60]. Future single-cell studies hold promise as a means to address these and other unanswered questions about the cellular heterogeneity amongst lymphocytes, and within individual cancers, so as to define the precise gene expression differences that underlie their differing cellular phenotypes *in vivo*.

Distinct types of B-ALL driven by *hMYC* and *mMyc*

MYC acts oncogenically in many ALL cases, and MYC is hyperactive in several other forms of cancer also [89], so it is not surprising that *hMYC* and *mMyc* can induce

ALL in several types of lymphocytes [60]. However, the human and mouse MYC oncoproteins in these transgenic fish are highly conserved (435 amino acids, ~92% identical, ~94% similar; Figure 5), and both lines regulate MYC using the same zebrafish *rag2* promoter, so it was surprising to discover that B-ALL in *hMYC* and *mMyc* fish are quite different. Specifically, *hMYC* B-ALL arise in *ighz*-lineage precursor B cells, whereas *mMyc* B-ALL occur in pro-B cells of the *ighm* lineage [60]. Unlike mammals which lack IgZ, expression of the zebrafish IgZ isotype does not occur by class switching. Instead, because of the configuration of the *D. rerio* immunoglobulin heavy chain (IgH) locus, during VDJ recombination zebrafish B cells must delete *ighz* sequences in order to express IgM [82]. Thus, when B cells commit to the IgM lineage, they lose their ability to express IgZ. As such, IgZ B cells, which are believed to primarily mediate mucosal immunity, can be viewed as an earlier stage in zebrafish B cell development that precedes IgM lineage commitment.

We used RNA-seq to profile gene expression in *hMYC ighz⁺* and *mMyc ighm⁺* B-ALL (Figure 6) [60]. We

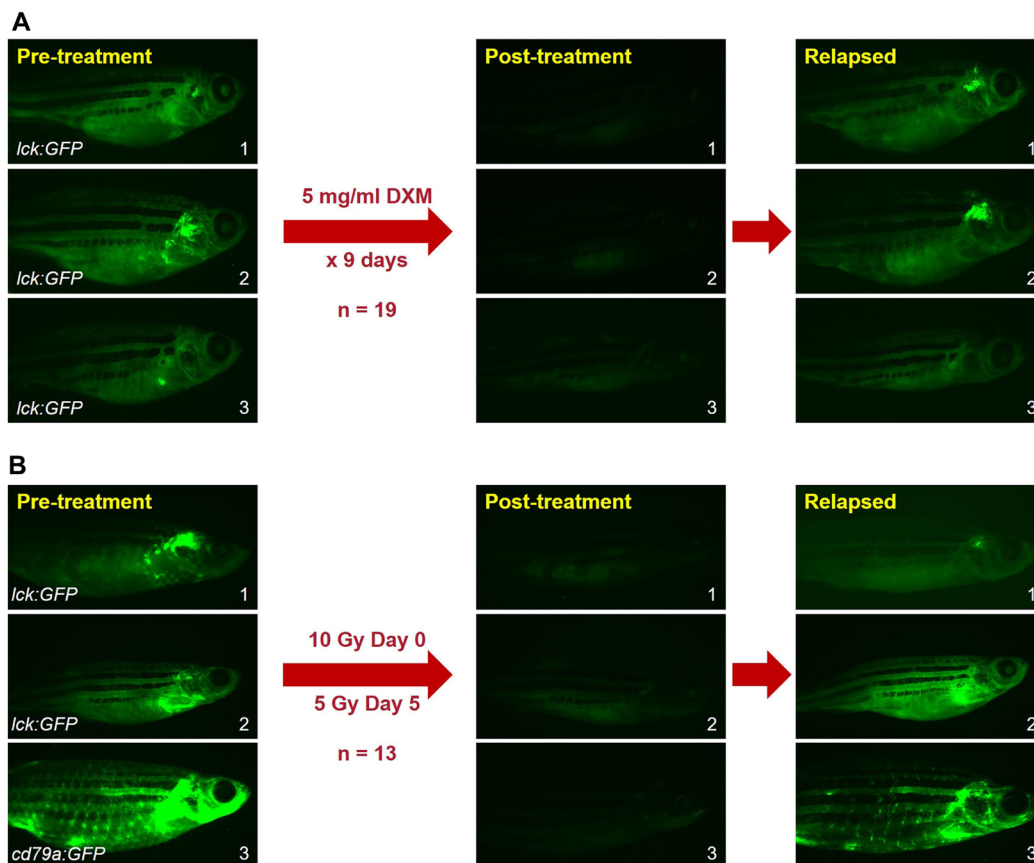


Figure 2: B-ALL regress with DXM or IR treatments. (A) B-ALL in *rag2:hMYC* fish treated with DXM for 9 days ($n = 19$). Post-treatment and relapsed images were obtained on days 9 and 28, respectively. Every (19/19) B-ALL regressed after DXM, but 11/19 (58%) B-ALL relapsed by day 28 (19 days after DXM withdrawal). (B) B-ALL in *rag2:hMYC* fish treated with IR ($n = 13$). Post-treatment and relapsed images were obtained on days 7 (i. e., 2 days after the 2nd IR dose) and 23, respectively. Every B-ALL (13/13) regressed after IR, but 100% recurred within 3 weeks of the 2nd IR dose. Upon relapse, flow cytometric testing (See Figure 1B) was used to verify that each relapse was GFP^{lo} B-ALL. Images of *rag2:hMYC, lck:GFP* fish (top 5 animals) have had brightness enhanced to facilitate visualization of dim B-ALL. Images of the *rag2:hMYC, cd79a:GFP* fish (lowest animal) are unmodified.

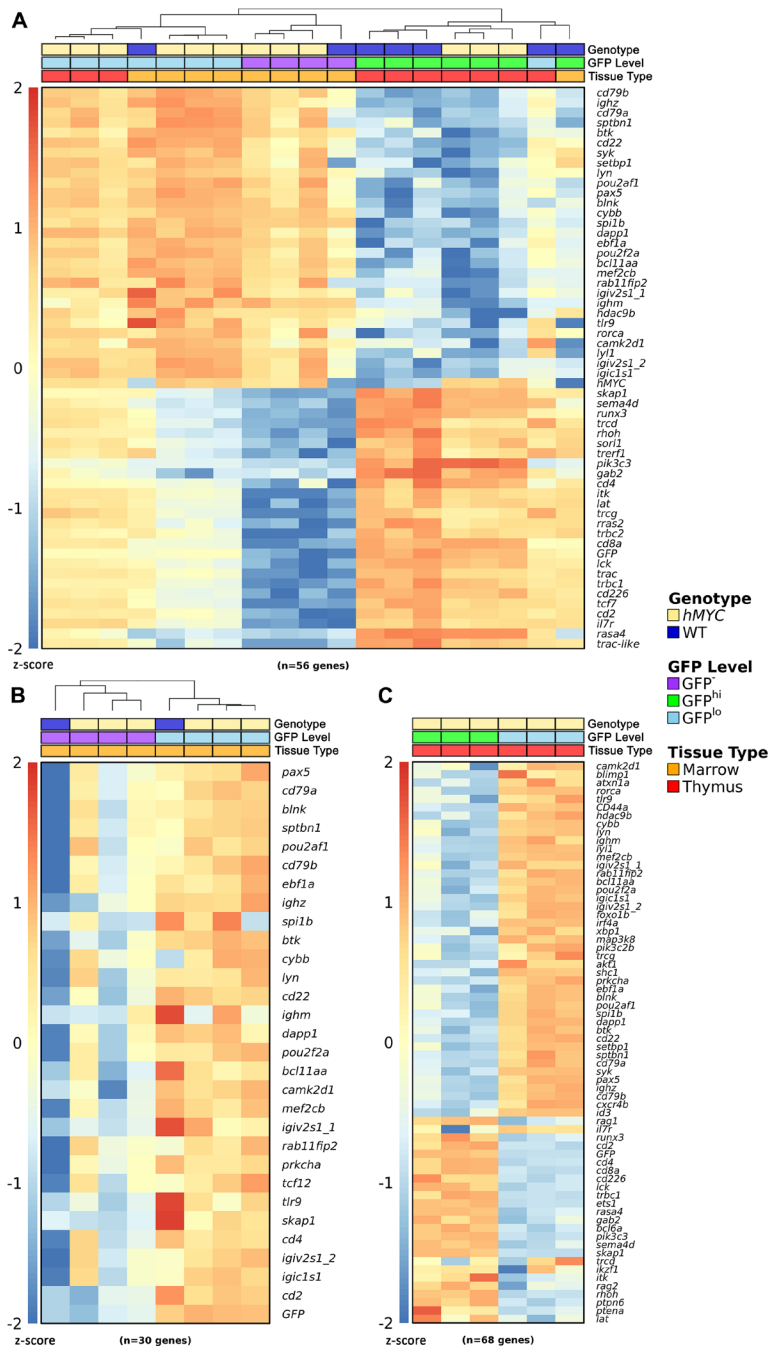


Figure 3: Gene expression in zebrafish lymphocytes. (A) Nanostring™ expression data in GFP^{hi}, GFP^{lo}, and GFP^{hi} lymphocytes from WT or *rag2:hMYC* fish bearing the *lck:GFP* marker transgene. *hMYC* GFP^{lo} cells from thymus and marrow express B cell genes, as do WT GFP^{lo} marrow cells. *hMYC* and WT GFP^{hi} marrow cells also express B cell transcripts. WT and *hMYC* GFP^{hi} thymocytes express T cells genes, as do WT GFP^{hi} marrow cells. WT GFP^{lo} thymocyte fractions contain a mixture of B and T cells (as do *hMYC* GFP^{lo} thymocytes and WT GFP^{lo} marrow cells), due to the difficulty of obtaining pure GFP^{lo} populations from these tissues [58, 63]. Samples are clustered hierarchically. (B) Nanostring™ expression data for B cell genes in marrow lymphocytes. WT and *hMYC* GFP^{lo} marrow cells show the strongest B cell signature, but B cell hyperplasia in *hMYC* fish increases the B cell signature of GFP^{hi} *hMYC* marrow cells compared to WT GFP^{lo} marrow cells, which show little-to-no B cell gene expression. Samples are clustered hierarchically. (C) Nanostring™ expression data in *hMYC* GFP^{lo} thymocytes express B, but not T, cell genes; *hMYC* GFP^{hi} thymocytes show the opposite pattern. In panels (A–C), triplicates [*hMYC*/GFP^{lo}/thymus (tan/lt. blue/red), *hMYC*/GFP^{lo}/marrow (tan/lt. blue/orange), *hMYC*/GFP^{hi}/marrow (tan/purple/orange), WT/GFP^{hi}/thymus (dk. blue/green/red), and *hMYC*/GFP^{hi}/thymus (tan/green/red)] represent individual biologic replicates, where each column depicts results from RNA of cells pooled from 10 fish. For each singleton sample [WT/GFP^{lo}/marrow (dk. blue/lt. blue/orange), WT/GFP^{hi}/marrow (dk. blue/purple/orange), WT/GFP^{lo}/thymus (dk. blue/lt. blue/red), and WT/GFP^{hi}/marrow (dk. blue/green/orange)], cells were pooled from 30 fish of the indicated genotype for RNA extraction. In panels A–C, read counts were log-transformed and converted to z-scores for visualization purposes. Scale bars are shown at the left of each heatmap.

compared 4 *hMYC* B-ALL to duplicate transcriptomes from the only 2 *mMyc* B-ALL thus far reported [57]. As noted, this revealed *hMYC* B-ALL expressed *ighz* constant regions while *mMyc* B-ALL expressed *ighm* constant region mRNA [60], plus additional differences. Overall,

> 400 genes displayed statistically-significant differential expression (Figure 6A and Supplementary Tables 2 and 3), including several pathways of interest. Curiously, in *hMYC* B-ALL much higher expression levels were seen for 9 of 10 *fos* and *jun* family members in the zebrafish

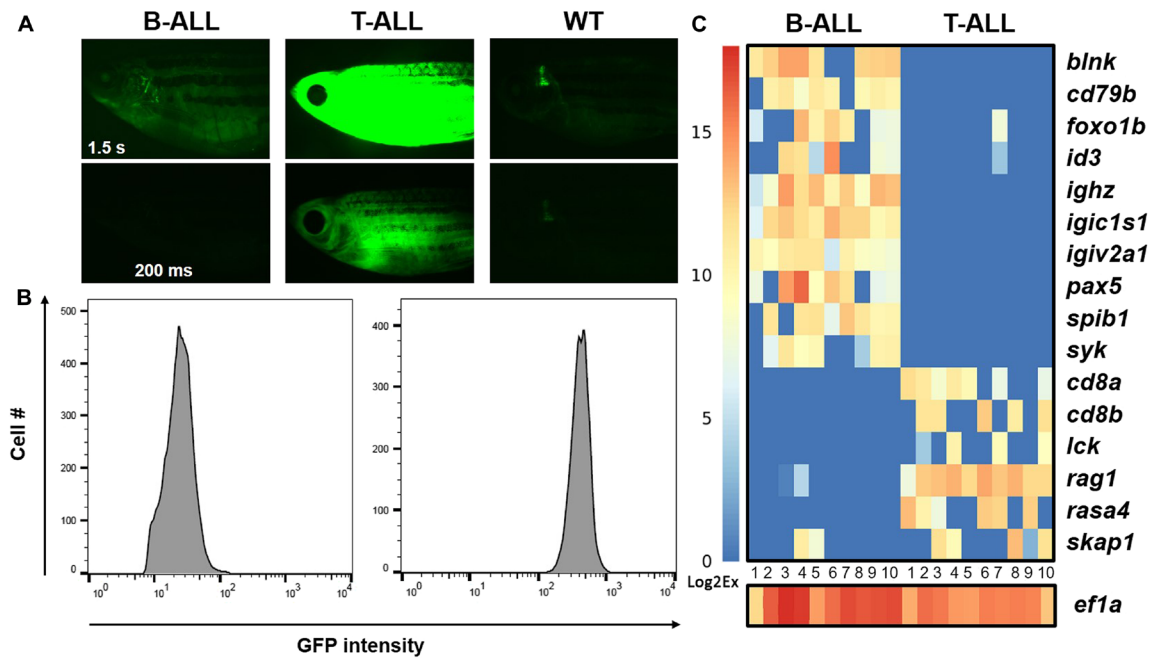


Figure 4: Gene expression in individual *hMYC* B- and T-ALL cells. (A) *rag2:hMYC;lck: GFP* fish with dim (left) and bright (center) cancers. B-ALL is only visible with 1.5 s exposure (upper left); T-ALL is visible with either 1.5 s (upper middle) or 200 ms (lower middle) exposures. Control *lck:GFP* fish images are shown at right, where only the thymus is visible. (B) Flow cytometry plots of the same ALL samples demonstrate GFP^{lo} B-ALL and GFP^{hi} T-ALL specimens. (C) Gene expression in single B- and T-ALL cells of the same cancers (*n* = 10 cells for each), as determined by Fluidigm™ Biomark qRT-PCR. B-ALL cells express B cell, but not T cell, genes; T-ALL show the opposite pattern. Expression of *ef1a111* (homologue of human *eukaryotic translation elongation factor 1 alpha 1*, aka *EF1A*) was used as a threshold control for the presence of RNA in each well. CT values were converted to Log2Ex for visualization (scale bar at left).

<i>hMYC</i>	1	MPLNV	SFTNRNYDL	LDYSVQPYF	Y	CDEEENFY	QQQQQSEL	QPPAPSED	IWKKFEL	55				
<i>mMyc</i>	1	MPLNV	NFTNRNYDL	LDYSVQPYF	I	CDEEENFY	HQQQQSEL	QPPAPSED	IWKKFEL	55				
<i>hMYC</i>	56	LPTPPLSP	RRSGLC	SPSYVAV	-	TPFSLRG	NDGGGGSF	STADQLEM	VTELLGGD	109				
<i>mMyc</i>	56	LPTPPLSP	RRSGLC	SPSYVAV	A	TSPSPRED	DDGGGGNF	STADQLEM	MTTELLGGD	110				
<i>hMYC</i>	110	MVNQSF	ICDPDETF	IKNII	I	QDCMWSGF	SAAAKLV	SEKCLASY	QAARKD	SGSPNP	164			
<i>mMyc</i>	111	MVNQSF	ICDPDETF	IKNII	I	QDCMWSGF	SAAAKLV	SEKCLASY	QAARKD	STSLSP	165			
<i>hMYC</i>	165	ARGHSVC	STSSLYL	LQDL	S	AAAASEC	IDPSVVF	PYPLND	SSSPKSC	ASQDSS	S	AFSPS	219	
<i>mMyc</i>	166	ARGHSVC	STSSLYL	LQDL	T	AAAASEC	IDPSVVF	PYPLND	SSSPKSC	TSSDST	AFSPS	220		
<i>hMYC</i>	220	SDSLLS	STESSPQ	G	S	PEPLVL	HEETPPT	TSSDSE	EEQEDEE	E	IVVSVE	KRQAP	G	274
<i>mMyc</i>	221	SDSLLS	-ESSPR	A	S	PEPLVL	HEETPPT	TSSDSE	EEQEDEE	E	IVVSVE	KRQTP	A	274
<i>hMYC</i>	275	KRSEGS	SPSAGG	HSKPPH	SPLVL	KRCHV	STHQHNY	AAPPSTR	KDYPA	AAKRV	KLDS	329		
<i>mMyc</i>	275	KRSEGS	SPSRG	HSKPPH	SPLVL	KRCHV	STHQHNY	AAPPSTR	KDYPA	AAKRA	KLDS	329		
<i>hMYC</i>	330	VRVLR	QISNNR	KCT	SPRSS	DTEEN	V	KRRTHN	VLERQR	RNELK	RSFFAL	RDQ	IPEL	384
<i>mMyc</i>	330	GRVLR	KQISNNR	KCS	SPRSS	DTEEN	D	KRRTHN	VLERQR	RNELK	RSFFAL	RDQ	IPEL	384
<i>hMYC</i>	385	ENNEKAP	KVVIL	KKATAY	ILS	VQAE	EEQKL	I	SEEDLL	RKRRE	QLKHK	LEQLR	435	
<i>mMyc</i>	385	ENNEKAP	KVVIL	KKATAY	ILS	IQA	DEHKL	TSEK	DLLR	KRRE	QLKHK	LEQLR	435	

Figure 5: Alignment of human and murine MYC proteins. Transgenic human and mouse MYC are 435 and 439 amino acids, respectively (last four *mMyc* residues not shown). Proteins show > 91% identity (399 residues, shaded light blue) and > 94% similarity (410 residues; 11 additional similar residues shaded darker blue).

genome (green bar in Figure 6A) with the lone exception *fosl1b*, which was higher in *mMyc* B-ALL. Also intriguing was the finding that all 6 endogenous *D. rerio* MYC family members (*myca*, *mycb*, *mycn*, *mych*, *mycla*, and *myclb*; red bar in Figure 6A) were more highly expressed in *hMYC*-driven B-ALL, as were multiple MYC-binding proteins and several MAX proteins, which heterodimerize with MYC (purple bar in Figure 6A).

B-ALL from the *mMyc* model showed dramatic up-regulation of many genes belonging to the Gene Ontology (GO) RNA binding pathway (blue bar in Figure 6A and top entry of Figure 6B lower panel). Several other genes also showed higher expression in *mMyc* B-ALL (Supplementary Table 3), including *D. rerio* homologues of mechanistic target of rapamycin kinase (*MTOR*) and the MTOR complex 1 member *RPTOR*,

multiple cyclin-dependent kinases and related cell cycle regulators (*CDK5*, *CDK14*, *CDC5L*, *CACUL1*, *TNK2*), and the non-receptor tyrosine phosphatases *PTPN13* and *PTPN21*. Together, these results suggest cell growth and division may be regulated differently in *mMyc* vs. *hMYC* B-ALL. Other notable orthologues up-regulated in *mMyc* B-ALL included the MYB-like gene *MYSM1*, two genes with jumonji lysine demethylase domains (*JMJD8*, *JARID2*), and the transcription factor *NFAT5*.

We postulate these and other differences may explain the apparently disparate oncogenic mechanisms employed by *hMYC* and *mMyc* in the B lymphoblasts of these closely-related lines. Pathway analysis of differentially-regulated genes predicted differing activation of several biologic pathways (e.g., cell differentiation, immune system process, lymphocyte activation, RNA binding, etc.; Figure

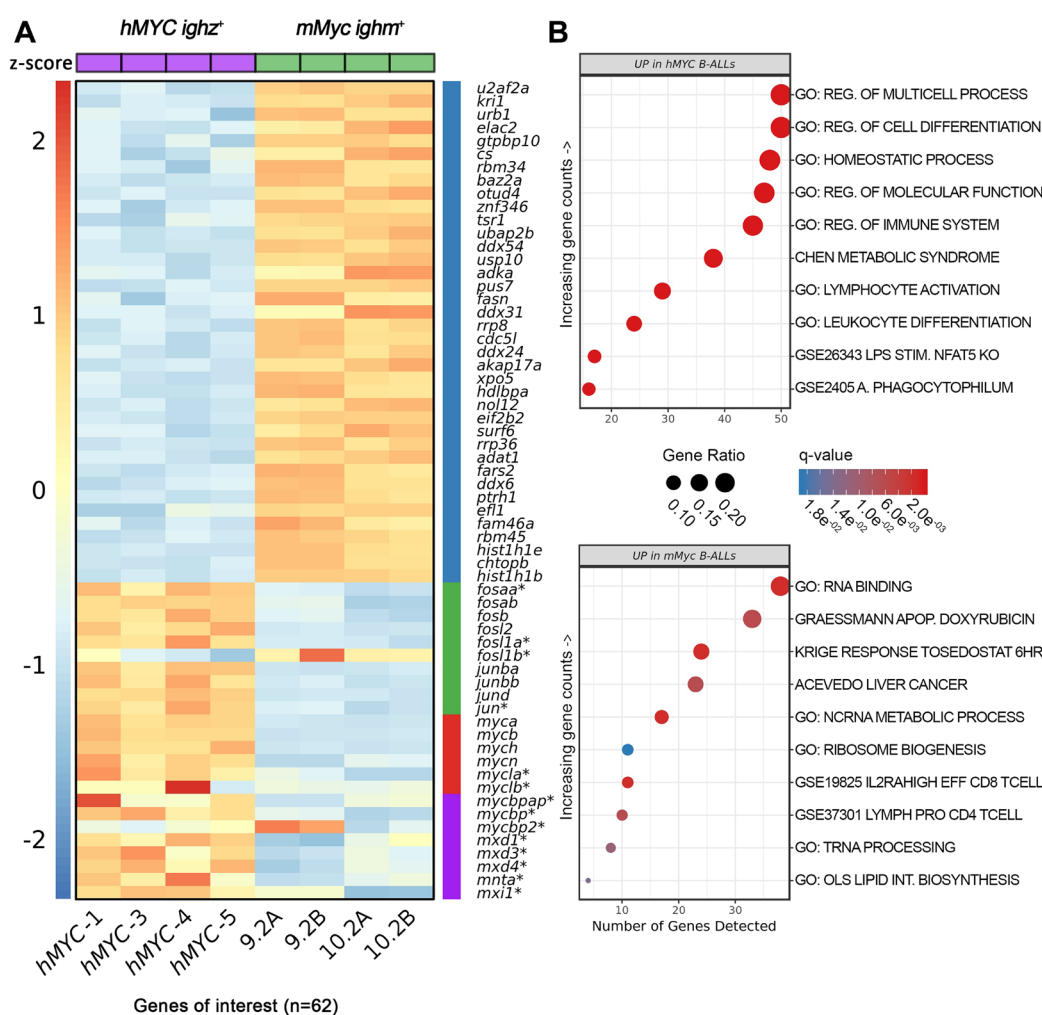


Figure 6: Differentially-expressed genes in *hMYC* versus *mMyc* B-ALL. (A) Heatmap depicting 62 differentially-expressed mRNA, including genes of the Gene Ontology (GO) RNA binding pathway (blue bar), *D. rerio fosl/jun*-family members (green bar), endogenous *myc*-family members (red bar), and other *myc*-related proteins, including several *max* heterodimeric partners (purple bar). Samples *hMYC*-1, -3, -4, and -5 are four distinct *hMYC* B-ALL; 9.2A/B and 10.2A/B pairs are RNA-seq technical replicates of two *mMyc* B-ALL [57, 60]. Genes not meeting differential expression testing thresholds or other filtering criteria are marked by asterisks (FDR < 0.05, absolute fold-change ≥ 1.5). Read counts are shown as z-scores (scale bar at left). (B) Top ten biologic pathways up-regulated in *hMYC* (top) or *mMyc* B-ALL (bottom; FDR < 0.05). Pathways are ordered according to the number of genes detected in the gene set (x-axis) and colored based on FDR *q*-value. Data point sizes correspond to the percentage of genes over-expressed in each pathway.

6B panels and Supplementary Table 4). These markedly different pathway signatures further demonstrate that human and murine MYC are far from synonymous in terms of their oncogenic effects upon zebrafish B lymphoblasts.

CONCLUSIONS

Recent discoveries of B-ALL in *D. rerio* lines previously-known to develop T-ALL were unexpected, but in retrospect, are not surprising. Both B and T lymphoblasts express *rag2*, so it is predictable that the transgenic promoters used in *hMYC* and *mMyc* fish would be active in both lymphocyte lineages. Likewise, MYC is known to be potentially oncogenic in multiple types of B cell cancer, so the fact that mammalian MYC proteins can induce zebrafish B-ALL is no more surprising than their already well-documented activities in promoting zebrafish T-ALL. Rather, what is somewhat surprising is that over a decade passed between the first description of *rag2:mMyc* fish and the recognition that B-ALL occurred in them. This may reflect that B-ALL is less prevalent than T-ALL, but our incidence data in the related *rag2:hMYC* line (Figure 1A) demonstrate that B-ALL is still quite common—at least in *hMYC* fish. Irrespective of this, now that B-ALL are described, recognizing them is straightforward, either by differential GFP expression in the *lck:GFP* background, or with other transgenic markers like *cd79a:GFP* or *cd79b:GFP* (Figure 1C). In the case of these latter two lines, T-ALL will of course still develop, but go undetected. In view of this, it is worth noting that other forms of ALL are perhaps yet to be discovered in *mMyc* and *hMYC* fish, as alluded to by the discovery of a biphenotypic ALL of mixed B/T-lineage in the aforementioned *mMyc* study [57]. Going forward, continued efforts to discern the molecular mechanisms by which MYC mediates oncogenic effects in different lymphocyte lineages promise to yield even more insights into how this potent oncogene can drive cancer in zebrafish, and in humans.

Author contributions

GP, JBG, CAF, CB, and JKF conceived and designed the study. GP, JBG, CB, and AH performed experiments. GP, JBG, CAF, CB, and JKF analyzed results. JKF wrote the manuscript, which all authors revised and approved.

ACKNOWLEDGMENTS AND FUNDING

We thank Megan-Malone Perez for zebrafish care, the Laboratory for Molecular Biology and Cytometry Research at OUHSC for use of their Core Facility, which assisted with FACS and Nanostring nCounter™ studies, and the Oklahoma Medical Research Foundation Clinical Genomics Center for assistance with Fluidigm Biomark™ multiplex qRT-PCR and RNA-seq. Research

reported in this publication was supported in part by the National Cancer Institute Cancer Center Support Grant P30CA225520 awarded to the University of Oklahoma Stephenson Cancer Center and used the Molecular Biology Shared Resource. The content is solely the responsibility of the authors and does not necessarily represent the official views of the National Institutes of Health. We also thank Sowmya Iyer, Sara Garcia, and David Langenau, Ph.D., at Massachusetts General Hospital and the Harvard Stem Cell Institute for their prior collaborative RNA-seq analyses. This work was supported by the OUHSC Jimmy Everest Section of Pediatric Hematology-Oncology, and grants from Hyundai Hope On Wheels, the Oklahoma Center for the Advancement of Science and Technology (HRP-067), and an INBRE pilot project award from the National Institute of General Medical Sciences (P20 GM103447). JKF holds the Children's Hospital Foundation E.L. & Thelma Gaylord Endowed Chair in Pediatric Hematology-Oncology.

CONFLICTS OF INTEREST

Authors declare no conflicts of interests.

REFERENCES

1. Pui CH, Yang JJ, Hunger SP, Pieters R, Schrappe M, Biondi A, Vora A, Baruchel A, Silverman LB, Schmiegelow K, Escherich G, Horibe K, Benoit YC, et al. Childhood Acute Lymphoblastic Leukemia: Progress Through Collaboration. *J Clin Oncol.* 2015; 33:2938–48. <https://doi.org/10.1200/JCO.2014.59.1636>. [PubMed]
2. Pui CH, Evans WE. A 50-year journey to cure childhood acute lymphoblastic leukemia. *Semin Hematol.* 2013; 50:185–96. <https://doi.org/10.1053/j.seminhematol.2013.06.007>. [PubMed]
3. Ward E, DeSantis C, Robbins A, Kohler B, Jemal A. Childhood and adolescent cancer statistics, 2014. *CA Cancer J Clin.* 2014; 64:83–103. <https://doi.org/10.3322/caac.21219>. [PubMed]
4. Jabbour E, O'Brien S, Konopleva M, Kantarjian H. New insights into the pathophysiology and therapy of adult acute lymphoblastic leukemia. *Cancer.* 2015; 121:2517–28. <https://doi.org/10.1002/cncr.29383>. [PubMed]
5. Jabbour E, Pui CH, Kantarjian H. Progress and Innovations in the Management of Adult Acute Lymphoblastic Leukemia. *JAMA Oncol.* 2018; 4:1413–20. <https://doi.org/10.1001/jamaoncol.2018.1915>. [PubMed]
6. Curtin SC, Minino AM, Anderson RN. Declines in Cancer Death Rates Among Children and Adolescents in the United States, 1999–2014. *NCHS Data Brief.* 2016; 257:1–8. [PubMed]
7. Locatelli F, Schrappe M, Bernardo ME, Rutella S. How I treat relapsed childhood acute lymphoblastic leukemia. *Blood.* 2012; 120:2807–16. <https://doi.org/10.1182/blood-2012-02-265884>. [PubMed]

8. Woo JS, Alberti MO, Tirado CA. Childhood B-acute lymphoblastic leukemia: a genetic update. *Exp Hematol Oncol.* 2014; 3:16. <https://doi.org/10.1186/2162-3619-3-16>. [PubMed]
9. Kohnken R, Porcu P, Mishra A. Overview of the Use of Murine Models in Leukemia and Lymphoma Research. *Front Oncol.* 2017; 7:22. <https://doi.org/10.3389/fonc.2017.00022>. [PubMed]
10. Jacoby E, Chien CD, Fry TJ. Murine models of acute leukemia: important tools in current pediatric leukemia research. *Front Oncol.* 2014; 4:95. <https://doi.org/10.3389/fonc.2014.00095>. [PubMed]
11. Letrado P, de Miguel I, Lamberto I, Diez-Martinez R, Oyarzabal J. Zebrafish: Speeding Up the Cancer Drug Discovery Process. *Cancer Res.* 2018; 78:6048–58. <https://doi.org/10.1158/0008-5472.CAN-18-1029>. [PubMed]
12. Leslie M. Zebrafish larvae could help to personalize cancer treatments. *Science.* 2017; 357:745. <https://doi.org/10.1126/science.357.6353.745>. [PubMed]
13. Kirchberger S, Sturtzel C, Pascoal S, Distel M. Quo natus, Danio?-Recent Progress in Modeling Cancer in Zebrafish. *Front Oncol.* 2017; 7:186. <https://doi.org/10.3389/fonc.2017.00186>. [PubMed]
14. Langenau DM, Sweet-Cordero A, Wechsler-Reya RJ, Dyer MA. Preclinical Models Provide Scientific Justification and Translational Relevance for Moving Novel Therapeutics into Clinical Trials for Pediatric Cancer. *Cancer Res.* 2015; 75:5176–86. <https://doi.org/10.1158/0008-5472.CAN-15-1308>. [PubMed]
15. Blackburn JS, Langenau DM. Zebrafish as a model to assess cancer heterogeneity, progression and relapse. *Dis Model Mech.* 2014; 7:755–62. <https://doi.org/10.1242/dmm.015842>. [PubMed]
16. White R, Rose K, Zon L. Zebrafish cancer: the state of the art and the path forward. *Nat Rev Cancer.* 2013; 13:624–36. <https://doi.org/10.1038/nrc3589>. [PubMed]
17. Howe K, Clark MD, Torroja CF, Torrance J, Berthelot C, Muffato M, Collins JE, Humphray S, McLaren K, Matthews L, McLaren S, Sealy I, Caccamo M, et al. The zebrafish reference genome sequence and its relationship to the human genome. *Nature.* 2013; 496:498–503. <https://doi.org/10.1038/nature12111>. [PubMed]
18. Zhuravleva J, Paggetti J, Martin L, Hammann A, Solary E, Bastie JN, Delva L. MOZ/TIF2-induced acute myeloid leukaemia in transgenic fish. *Br J Haematol.* 2008; 143:378–82. <https://doi.org/10.1111/j.1365-2141.2008.07362.x>. [PubMed]
19. Yeh JR, Munson KM, Chao YL, Peterson QP, Macrae CA, Peterson RT. AML1-ETO reprograms hematopoietic cell fate by downregulating scl expression. *Development.* 2008; 135:401–10. <https://doi.org/10.1242/dev.008904>. [PubMed]
20. Bolli N, Payne EM, Grabher C, Lee JS, Johnston AB, Falini B, Kanki JP, Look AT. Expression of the cytoplasmic NPM1 mutant (NPMc+) causes the expansion of hematopoietic cells in zebrafish. *Blood.* 2010; 115:3329–40. <https://doi.org/10.1182/blood-2009-02-207225>. [PubMed]
21. Dayyani F, Wang J, Yeh JR, Ahn EY, Tobey E, Zhang DE, Bernstein ID, Peterson RT, Sweetser DA. Loss of TLE1 and TLE4 from the del(9q) commonly deleted region in AML cooperates with AML1-ETO to affect myeloid cell proliferation and survival. *Blood.* 2008; 111:4338–47. <https://doi.org/10.1182/blood-2007-07-103291>. [PubMed]
22. Shen LJ, Chen FY, Zhang Y, Cao LF, Kuang Y, Zhong M, Wang T, Zhong H. MYCN transgenic zebrafish model with the characterization of acute myeloid leukemia and altered hematopoiesis. *PLoS One.* 2013; 8:e59070. <https://doi.org/10.1371/journal.pone.0059070>. [PubMed]
23. Zhang Y, Wang J, Wheat J, Chen X, Jin S, Sadrzadeh H, Fathi AT, Peterson RT, Kung AL, Sweetser DA, Yeh JR. AML1-ETO mediates hematopoietic self-renewal and leukemogenesis through a COX/beta-catenin signaling pathway. *Blood.* 2013; 121:4906–16. <https://doi.org/10.1182/blood-2012-08-447763>. [PubMed]
24. Forrester AM, Grabher C, McBride ER, Boyd ER, Vigerstad MH, Edgar A, Kai FB, Da'as SI, Payne E, Look AT, Berlan JN. NUP98-HOXA9-transgenic zebrafish develop a myeloproliferative neoplasm and provide new insight into mechanisms of myeloid leukaemogenesis. *Br J Haematol.* 2011; 155:167–81. <https://doi.org/10.1111/j.1365-2141.2011.08810.x>. [PubMed]
25. Yeh JR, Munson KM, Elagib KE, Goldfarb AN, Sweetser DA, Peterson RT. Discovering chemical modifiers of oncogene-regulated hematopoietic differentiation. *Nat Chem Biol.* 2009; 5:236–43. <https://doi.org/nchembio.147>. [PubMed]
26. Alghisi E, Distel M, Malagola M, Anelli V, Santoriello C, Herwig L, Krudewig A, Henkel CV, Russo D, Mione MC. Targeting oncogene expression to endothelial cells induces proliferation of the myelo-erythroid lineage by repressing the Notch pathway. *Leukemia.* 2013; 27:2229–41. <https://doi.org/10.1038/leu.2013.132>. [PubMed]
27. Feng H, Langenau DM, Madge JA, Quinkertz A, Gutierrez A, Neuberg DS, Kanki JP, Look AT. Heat-shock induction of T-cell lymphoma/leukaemia in conditional Cre/lox-regulated transgenic zebrafish. *Br J Haematol.* 2007; 138:169–75. <https://doi.org/10.1111/j.1365-2141.2007.06625.x>. [PubMed]
28. Feng H, Stachura DL, White RM, Gutierrez A, Zhang L, Sanda T, Jette CA, Testa JR, Neuberg DS, Langenau DM, Kutok JL, Zon LI, Traver D, et al. T-lymphoblastic lymphoma cells express high levels of BCL2, S1P1, and ICAM1, leading to a blockade of tumor cell intravasation. *Cancer Cell.* 2010; 18:353–66. <https://doi.org/10.1016/j.ccr.2010.09.009>. [PubMed]
29. Langenau DM, Traver D, Ferrando AA, Kutok JL, Aster JC, Kanki JP, Lin S, Prochownik E, Trede NS, Zon LI, Look AT. Myc-induced T cell leukemia in transgenic zebrafish. *Science.* 2003; 299:887–90. <https://doi.org/10.1126/science.1080280>. [PubMed]

30. Langenau DM, Feng H, Berghmans S, Kanki JP, Kutok JL, Look AT. Cre/lox-regulated transgenic zebrafish model with conditional myc-induced T cell acute lymphoblastic leukemia. *Proc Natl Acad Sci U S A*. 2005; 102:6068–73. <https://doi.org/10.1073/pnas.0408708102>. [PubMed]
31. Frazer JK, Meeker ND, Rudner L, Bradley DF, Smith AC, Demarest B, Joshi D, Locke EE, Hutchinson SA, Tripp S, Perkins SL, Trede NS. Heritable T-cell malignancy models established in a zebrafish phenotypic screen. *Leukemia*. 2009; 23:1825–35. <https://doi.org/10.1038/leu.2009.116>. [PubMed]
32. Gutierrez A, Grebliunaite R, Feng H, Kozakewich E, Zhu S, Guo F, Payne E, Mansour M, Dahlberg SE, Neuberg DS, den Hertog J, Prochownik EV, Testa JR, et al. Pten mediates Myc oncogene dependence in a conditional zebrafish model of T cell acute lymphoblastic leukemia. *J Exp Med*. 2011; 208:1595–603. <https://doi.org/10.1084/jem.20101691>. [PubMed]
33. Reynolds C, Roderick JE, LaBelle JL, Bird G, Mathieu R, Bodaar K, Colon D, Pyati U, Stevenson KE, Qi J, Harris M, Silverman LB, Sallan SE, et al. Repression of BIM mediates survival signaling by MYC and AKT in high-risk T-cell acute lymphoblastic leukemia. *Leukemia*. 2014; 28:1819–27. <https://doi.org/10.1038/leu.2014.78>. [PubMed]
34. Anderson NM, Li D, Peng HL, Laroche FJ, Mansour MR, Gjini E, Aioub M, Helman DJ, Roderick JE, Cheng T, Harrold I, Samaha Y, Meng L, et al. The TCA cycle transferase DLST is important for MYC-mediated leukemogenesis. *Leukemia*. 2016; 30:1365–74. <https://doi.org/10.1038/leu.2016.26>. [PubMed]
35. Huiting LN, Samaha Y, Zhang GL, Roderick JE, Li B, Anderson NM, Wang YW, Wang L, Laroche F, Choi JW, Liu CT, Kelliher MA, Feng H. UFD1 contributes to MYC-mediated leukemia aggressiveness through suppression of the proapoptotic unfolded protein response. *Leukemia*. 2018; 32:2339–2351. <https://doi.org/10.1038/s41375-018-0141-x>. [PubMed]
36. Chen J, Jette C, Kanki JP, Aster JC, Look AT, Griffin JD. NOTCH1-induced T-cell leukemia in transgenic zebrafish. *Leukemia*. 2007; 21:462–71. <https://doi.org/10.1038/sj.leu.2404546>. [PubMed]
37. Mansour MR, He S, Li Z, Lobbardi R, Abraham BJ, Hug C, Rahman S, Leon TE, Kuang YY, Zimmerman MW, Blonquist T, Gjini E, Gutierrez A, et al. JDP2: An oncogenic bZIP transcription factor in T cell acute lymphoblastic leukemia. *J Exp Med*. 2018; 215:1929–45. <https://doi.org/10.1084/jem.20170484>. [PubMed]
38. Rudner LA, Brown KH, Dobrinski KP, Bradley DF, Garcia MI, Smith AC, Downie JM, Meeker ND, Look AT, Downing JR, Gutierrez A, Mullighan CG, Schiffman JD, et al. Shared acquired genomic changes in zebrafish and human T-ALL. *Oncogene*. 2011; 30:4289–96. <https://doi.org/10.1038/onc.2011.138>. [PubMed]
39. Blackburn JS, Liu S, Wilder JL, Dobrinski KP, Lobbardi R, Moore FE, Martinez SA, Chen EY, Lee C, Langenau DM. Clonal evolution enhances leukemia-propagating cell frequency in T cell acute lymphoblastic leukemia through Akt/mTORC1 pathway activation. *Cancer Cell*. 2014; 25:366–78. <https://doi.org/10.1016/j.ccr.2014.01.032>. [PubMed]
40. Blackburn JS, Liu S, Raiser DM, Martinez SA, Feng H, Meeker ND, Gentry J, Neuberg D, Look AT, Ramaswamy S, Bernards A, Trede NS, Langenau DM. Notch signaling expands a pre-malignant pool of T-cell acute lymphoblastic leukemia clones without affecting leukemia-propagating cell frequency. *Leukemia*. 2012; 26:2069–78. <https://doi.org/10.1038/leu.2012.116>. [PubMed]
41. Gutierrez A, Feng H, Stevenson K, Neuberg DS, Calzada O, Zhou Y, Langenau DM, Look AT. Loss of function tp53 mutations do not accelerate the onset of myc-induced T-cell acute lymphoblastic leukaemia in the zebrafish. *Br J Haematol*. 2014; 166:84–90. <https://doi.org/10.1111/bjh.12851>. [PubMed]
42. Lobbardi R, Pinder J, Martinez-Pastor B, Theodorou M, Blackburn JS, Abraham BJ, Namiki Y, Mansour M, Abdelfattah NS, Molodtsov A, Alexe G, Toiber D, de Waard M, et al. TOX Regulates Growth, DNA Repair, and Genomic Instability in T-cell Acute Lymphoblastic Leukemia. *Cancer Discov*. 2017; 7:1336–53. <https://doi.org/10.1158/2159-8290.CD-17-0267>. [PubMed]
43. Ridges S, Heaton WL, Joshi D, Choi H, Eiring A, Batchelor L, Choudhry P, Manos EJ, Sofla H, Sanati A, Welborn S, Agarwal A, Spangrude GJ, et al. Zebrafish screen identifies novel compound with selective toxicity against leukemia. *Blood*. 2012; 119:5621–31. <https://doi.org/10.1182/blood-2011-12-398818>. [PubMed]
44. Gutierrez A, Pan L, Groen RW, Baleyrier F, Kentsis A, Marineau J, Grebliunaite R, Kozakewich E, Reed C, Pflumio F, Poglio S, Uzan B, Clemons P, et al. Phenothiazines induce PP2A-mediated apoptosis in T cell acute lymphoblastic leukemia. *J Clin Invest*. 2014; 124:644–55. <https://doi.org/10.1172/JCI65093>. [PubMed]
45. Tang Q, Moore JC, Ignatius MS, Tenente IM, Hayes MN, Garcia EG, Torres Yordan N, Bourque C, He S, Blackburn JS, Look AT, Houvras Y, Langenau DM. Imaging tumour cell heterogeneity following cell transplantation into optically clear immune-deficient zebrafish. *Nat Commun*. 2016; 7:10358. <https://doi.org/10.1038/ncomms10358>. [PubMed]
46. Langenau DM, Jette C, Berghmans S, Palomero T, Kanki JP, Kutok JL, Look AT. Suppression of apoptosis by bcl-2 overexpression in lymphoid cells of transgenic zebrafish. *Blood*. 2005; 105:3278–85. <https://doi.org/10.1182/blood-2004-08-3073>. [PubMed]
47. Smith AC, Raimondi AR, Salthouse CD, Ignatius MS, Blackburn JS, Mizgirev IV, Storer NY, de Jong JL, Chen AT, Zhou Y, Revskoy S, Zon LI, Langenau DM. High-throughput cell transplantation establishes that tumor-initiating cells are abundant in zebrafish T-cell acute lymphoblastic leukemia. *Blood*. 2010; 115:3296–303. <https://doi.org/10.1182/blood-2009-10-246488>. [PubMed]
48. Moore FE, Garcia EG, Lobbardi R, Jain E, Tang Q, Moore JC, Cortes M, Molodtsov A, Kasheta M, Luo CC,

- Garcia AJ, Mylvaganam R, Yoder JA, et al. Single-cell transcriptional analysis of normal, aberrant, and malignant hematopoiesis in zebrafish. *J Exp Med*. 2016; 213:979–92. <https://doi.org/10.1084/jem.20152013>. [PubMed]
49. Tang Q, Iyer S, Lobbardi R, Moore JC, Chen H, Lareau C, Hebert C, Shaw ML, Neftel C, Suva ML, Ceol CJ, Bernards A, Aryee M, et al. Dissecting hematopoietic and renal cell heterogeneity in adult zebrafish at single-cell resolution using RNA sequencing. *J Exp Med*. 2017; 214:2875–87. <https://doi.org/10.1084/jem.20170976>. [PubMed]
 50. Baeten JT, Waarts MR, Pruitt MM, Chan WC, Andrade J, de Jong JLO. The side population enriches for leukemia propagating cell activity and Wnt pathway expression in zebrafish acute lymphoblastic leukemia. *Haematologica*. 2019; 104:1388–1395. <https://doi.org/10.3324/haematol.2018.206417>. [PubMed]
 51. Leong WZ, Tan SH, Ngoc PCT, Amanda S, Yam AWY, Liau WS, Gong Z, Lawton LN, Tenen DG, Sanda T. ARID5B as a critical downstream target of the TAL1 complex that activates the oncogenic transcriptional program and promotes T-cell leukemogenesis. *Genes Dev*. 2017; 31:2343–60. <https://doi.org/10.1101/gad.302646.117>. [PubMed]
 52. Liau WS, Tan SH, Ngoc PCT, Wang CQ, Tergaonkar V, Feng H, Gong Z, Osato M, Look AT, Sanda T. Aberrant activation of the GIMAP enhancer by oncogenic transcription factors in T-cell acute lymphoblastic leukemia. *Leukemia*. 2017; 31:1798–807. <https://doi.org/10.1038/leu.2016.392>. [PubMed]
 53. Li Z, He S, Look AT. The MCL1-specific inhibitor S63845 acts synergistically with venetoclax/ABT-199 to induce apoptosis in T-cell acute lymphoblastic leukemia cells. *Leukemia*. 2019; 33:262–6. <https://doi.org/10.1038/s41375-018-0201-2>. [PubMed]
 54. Sabaawy HE, Azuma M, Embree LJ, Tsai HJ, Starost MF, Hickstein DD. TEL-AML1 transgenic zebrafish model of precursor B cell acute lymphoblastic leukemia. *Proc Natl Acad Sci U S A*. 2006; 103:15166–71. <https://doi.org/10.1073/pnas.0603349103>. [PubMed]
 55. He S, Jing CB, Look AT. Zebrafish models of leukemia. *Methods Cell Biol*. 2017; 138:563–92. <https://doi.org/10.1016/bs.mcb.2016.11.013>. [PubMed]
 56. Squiban B, Frazer JK. Danio rerio: Small Fish Making a Big Splash in Leukemia. *Curr Pathobiol Rep*. 2014; 2:61–73. <https://doi.org/10.1007/s40139-014-0041-3>. [PubMed]
 57. Garcia EG, Iyer S, Garcia SP, Loontjens S, Sadreyev RI, Speleman F, Langenau DM. Cell of origin dictates aggression and stem cell number in acute lymphoblastic leukemia. *Leukemia*. 2018; 32:1860–5. <https://doi.org/10.1038/s41375-018-0130-0>. [PubMed]
 58. Borga C, Park G, Foster C, Burroughs-Garcia J, Marchesin M, Shah R, Hasan A, Ahmed ST, Bresolin S, Batchelor L, Scordino T, Miles RR, Te Kronnie G, et al. Simultaneous B and T cell acute lymphoblastic leukemias in zebrafish driven by transgenic MYC: implications for oncogenesis and lymphopoiesis. *Leukemia*. 2019; 33:333–47. <https://doi.org/10.1038/s41375-018-0226-6>. [PubMed]
 59. Langenau DM, Ferrando AA, Traver D, Kutok JL, Hezel JP, Kanki JP, Zon LI, Look AT, Trede NS. *In vivo* tracking of T cell development, ablation, and engraftment in transgenic zebrafish. *Proc Natl Acad Sci U S A*. 2004; 101:7369–74. <https://doi.org/10.1073/pnas.0402248101>. [PubMed]
 60. Borga C, Foster CA, Iyer S, Garcia SP, Langenau DM, Frazer JK. Molecularly distinct models of zebrafish Myc-induced B cell leukemia. *Leukemia*. 2019; 33:559–62. <https://doi.org/10.1038/s41375-018-0328-1>. [PubMed]
 61. Liu X, Li YS, Shinton SA, Rhodes J, Tang L, Feng H, Jette CA, Look AT, Hayakawa K, Hardy RR. Zebrafish B Cell Development without a Pre-B Cell Stage, Revealed by CD79 Fluorescence Reporter Transgenes. *J Immunol*. 2017; 199:1706–15. <https://doi.org/10.4049/jimmunol.1700552>. [PubMed]
 62. Traver D, Paw BH, Poss KD, Penberthy WT, Lin S, Zon LI. Transplantation and *in vivo* imaging of multilineage engraftment in zebrafish bloodless mutants. *Nat Immunol*. 2003; 4:1238–46. <https://doi.org/10.1038/ni1007>. [PubMed]
 63. Burroughs-Garcia J, Hasan A, Park G, Borga C, Frazer JK. Isolating Malignant and Non-Malignant B Cells from lck:eGFP Zebrafish. *J Vis Exp*. 2019; 144:e59191. <https://doi.org/10.3791/59191>. [PubMed]
 64. Christoph S, Deryckere D, Schlegel J, Frazer JK, Batchelor LA, Trakhimets AY, Sather S, Hunter DM, Cummings CT, Liu J, Yang C, Kireev D, Simpson C, et al. UNC569, a novel small-molecule mer inhibitor with efficacy against acute lymphoblastic leukemia *in vitro* and *in vivo*. *Mol Cancer Ther*. 2013; 12:2367–77. <https://doi.org/10.1158/1535-7163.MCT-13-0040>. [PubMed]
 65. Dobin A, Davis CA, Schlesinger F, Drenkow J, Zaleski C, Jha S, Batut P, Chaisson M, Gingeras TR. STAR: ultrafast universal RNA-seq aligner. *Bioinformatics*. 2013; 29:15–21. <https://doi.org/10.1093/bioinformatics/bts635>. [PubMed]
 66. Zerbino DR, Achuthan P, Akanni W, Amode MR, Barrell D, Bhai J, Billis K, Cummins C, Gall A, Giron CG, Gil L, Gordon L, Haggerty L, et al. Ensembl 2018. *Nucleic Acids Res*. 2018; 46:D754–D61. <https://doi.org/10.1093/nar/gkx1098>. [PubMed]
 67. Liao Y, Smyth GK, Shi W. featureCounts: an efficient general purpose program for assigning sequence reads to genomic features. *Bioinformatics*. 2014; 30:923–30. <https://doi.org/10.1093/bioinformatics/btt656>. [PubMed]
 68. Love MI, Huber W, Anders S. Moderated estimation of fold change and dispersion for RNA-seq data with DESeq2. *Genome Biol*. 2014; 15:550. <https://doi.org/10.1186/s13059-014-0550-8>. [PubMed]
 69. Yu G, Wang LG, Han Y, He QY. clusterProfiler: an R package for comparing biological themes among gene clusters. *OMICS*. 2012; 16:284–7. <https://doi.org/10.1089/omi.2011.0118>. [PubMed]
 70. Liberzon A, Subramanian A, Pinchback R, Thorvaldsdottir H, Tamayo P, Mesirov JP. Molecular signatures database (MSigDB) 3.0. *Bioinformatics*. 2011; 27:1739–40. <https://doi.org/10.1093/bioinformatics/btr260>. [PubMed]

71. Childhood Acute Lymphoblastic Leukemia Treatment (PDQ(R)): Health Professional Version. PDQ Cancer Information Summaries. (Bethesda (MD)). 2002.
72. Adult Acute Lymphoblastic Leukemia Treatment (PDQ(R)): Health Professional Version. PDQ Cancer Information Summaries. (Bethesda (MD)). 2002.
73. Shah DS, Kumar R. Steroid resistance in leukemia. *World J Exp Med.* 2013; 3:21–5. <https://doi.org/10.5493/wjem.v3.i2.21>. [PubMed]
74. Hochberg J, Cairo MS. Tumor lysis syndrome: current perspective. *Haematologica.* 2008; 93:9–13. <https://doi.org/10.3324/haematol.12327>. [PubMed]
75. Novershtern N, Subramanian A, Lawton LN, Mak RH, Haining WN, McConkey ME, Habib N, Yosef N, Chang CY, Shay T, Frampton GM, Drake AC, Leskov I, et al. Densely interconnected transcriptional circuits control cell states in human hematopoiesis. *Cell.* 2011; 144:296–309. <https://doi.org/10.1016/j.cell.2011.01.004>. [PubMed]
76. Haferlach T, Kohlmann A, Wiczorek L, Basso G, Kronnie GT, Bene MC, De Vos J, Hernandez JM, Hofmann WK, Mills KI, Gilkes A, Chiaretti S, Shurtleff SA, et al. Clinical utility of microarray-based gene expression profiling in the diagnosis and subclassification of leukemia: report from the International Microarray Innovations in Leukemia Study Group. *J Clin Oncol.* 2010; 28:2529–37. <https://doi.org/10.1200/JCO.2009.23.4732>. [PubMed]
77. Geiss GK, Bumgarner RE, Birditt B, Dahl T, Dowidar N, Dunaway DL, Fell HP, Ferree S, George RD, Grogan T, James JJ, Maysuria M, Mitton JD, et al. Direct multiplexed measurement of gene expression with color-coded probe pairs. *Nat Biotechnol.* 2008; 26:317–25. <https://doi.org/10.1038/nbt1385>. [PubMed]
78. Malkov VA, Serikawa KA, Balantac N, Watters J, Geiss G, Mashadi-Hosseini A, Fare T. Multiplexed measurements of gene signatures in different analytes using the Nanostring nCounter Assay System. *BMC Res Notes.* 2009; 2:80. <https://doi.org/10.1186/1756-0500-2-80>. [PubMed]
79. Palmer C, Diehn M, Alizadeh AA, Brown PO. Cell-type specific gene expression profiles of leukocytes in human peripheral blood. *BMC Genomics.* 2006; 7:115. <https://doi.org/10.1186/1471-2164-7-115>. [PubMed]
80. Carmona SJ, Teichmann SA, Ferreira L, Macaulay IC, Stubbington MJ, Cvejic A, Gfeller D. Single-cell transcriptome analysis of fish immune cells provides insight into the evolution of vertebrate immune cell types. *Genome Res.* 2017; 27:451–61. <https://doi.org/10.1101/gr.207704.116>. [PubMed]
81. Hernandez PP, Strzelecka PM, Athanasiadis EI, Hall D, Robalo AF, Collins CM, Boudinot P, Levraud JP, Cvejic A. Single-cell transcriptional analysis reveals ILC-like cells in zebrafish. *Sci Immunol.* 2018; 3. <https://doi.org/10.1126/sciimmunol.aau5265>. [PubMed]
82. Fillatreau S, Six A, Magadan S, Castro R, Sunyer JO, Boudinot P. The astonishing diversity of Ig classes and B cell repertoires in teleost fish. *Front Immunol.* 2013; 4:28. <https://doi.org/10.3389/fimmu.2013.00028>. [PubMed]
83. Castro R, Jouneau L, Pham HP, Bouchez O, Giudicelli V, Lefranc MP, Quillet E, Benmansour A, Cazals F, Six A, Fillatreau S, Sunyer O, Boudinot P. Teleost fish mount complex clonal IgM and IgT responses in spleen upon systemic viral infection. *PLoS Pathog.* 2013; 9:e1003098. <https://doi.org/10.1371/journal.ppat.1003098>. [PubMed]
84. Page DM, Wittamer V, Bertrand JY, Lewis KL, Pratt DN, Delgado N, Schale SE, McGue C, Jacobsen BH, Doty A, Pao Y, Yang H, Chi NC, et al. An evolutionarily conserved program of B-cell development and activation in zebrafish. *Blood.* 2013; 122:e1–11. <https://doi.org/10.1182/blood-2012-12-471029>. [PubMed]
85. Zhang H, Fei C, Wu H, Yang M, Liu Q, Wang Q, Zhang Y. Transcriptome profiling reveals Th17-like immune responses induced in zebrafish bath-vaccinated with a live attenuated *Vibrio anguillarum*. *PLoS One.* 2013; 8:e73871. <https://doi.org/10.1371/journal.pone.0073871>. [PubMed]
86. Sugimoto K, Hui SP, Sheng DZ, Nakayama M, Kikuchi K. Zebrafish FOXP3 is required for the maintenance of immune tolerance. *Dev Comp Immunol.* 2017; 73:156–62. <https://doi.org/10.1016/j.dci.2017.03.023>. [PubMed]
87. Hui SP, Sheng DZ, Sugimoto K, Gonzalez-Rajal A, Nakagawa S, Hesselson D, Kikuchi K. Zebrafish Regulatory T Cells Mediate Organ-Specific Regenerative Programs. *Dev Cell.* 2017; 43:659–72 e5. <https://doi.org/10.1016/j.devcel.2017.11.010>. [PubMed]
88. Cernan M, Sztokowski T, Pikalova Z. Mixed-phenotype acute leukemia: state-of-the-art of the diagnosis, classification and treatment. *Biomed Pap Med Fac Univ Palacky Olomouc Czech Repub.* 2017; 161:234–41. <https://doi.org/10.5507/bp.2017.013>. [PubMed]
89. Dang CV. MYC on the path to cancer. *Cell.* 2012; 149:22–35. <https://doi.org/10.1016/j.cell.2012.03.003>. [PubMed]